Japanese Journal of Applied Physics

STAP ARTICLE

Radiation resistance of praseodymium-doped aluminum lithium fluorophosphate scintillator glasses for laser fusion experiments

To cite this article: Keito Shinohara *et al* 2023 *Jpn. J. Appl. Phys.* **62** 010613

Radiation resistance of praseodymium-doped aluminum lithium fluorophosphate scintillator glasses for laser fusion experiments

Keito Shinohara[1*], Melvin John F. Empizo[1,2], Marilou Cadatal-Raduban[1,3], Kohei Yamanoi[1], Toshihiko Shimizu[1], Masashi Yoshimura[1], Nobuhiko Sarukura[1,4], Takahiro Murata[5], Mayrene A. Uy[1,6,7], Hitoshi Abe[6,7,8], Akira Yoshikawa[4,9], Georges Boulon[10], and Christophe Dujardin[10]

[1]*Institute of Laser Engineering, Osaka University, 2-6 Yamadaoka, Suita, Osaka 565-0871, Japan*
[2]*National Institute of Physics, University of the Philippines Diliman, Diliman, Quezon City 1101, Philippines*
[3]*Centre for Theoretical Chemistry and Physics, School of Natural Sciences, Massey University, Auckland 0632, New Zealand*
[4]*New Industry Creation Hatchery Center, Tohoku University. 6-6-10 Aoba, Aramaki, Aoba-ku, Sendai, Miyagi 980-8579, Japan*
[5]*Faculty of Advanced Science and Technology, Kumamoto University, 2-40-1 Kurokami, Chuo-ku, Kumamoto 860-8555, Japan*
[6]*Department of Materials Structure Science, School of High Energy Accelerator Science, The Graduate University for Advanced Studies (SOKENDAI), 1-1 Oho, Tsukuba, Ibaraki 305-0801, Japan*
[7]*Institute of Materials Structure Science (IMSS), High Energy Accelerator Research Organization (KEK), 1-1 Oho, Tsukuba, Ibaraki 305-0801, Japan*
[8]*Graduate School of Science and Engineering, Ibaraki University, 2-1-1 Bunkyo, Mito, Ibaraki 310-8512, Japan*
[9]*Institute of Multidisciplinary Research for Advanced Materials, Tohoku University, 2-1-1 Katahira, Aoba-ku, Sendai, Miyagi 980-8577, Japan*
[10]*Institut Lumière Matière, Univ Lyon, Université Claude Bernard Lyon 1, CNRS, Villeurbanne F-69622, France*

*E-mail: shinohara-k@ile.osaka-u.ac.jp

Received August 8, 2022; revised October 7, 2022; accepted November 7, 2022; published online December 2, 2022

We report the gamma (γ)-ray radiation resistance of praseodymium (Pr^{3+})-doped aluminum lithium fluorophosphate scintillator glasses. For its assessment as a scintillator material for laser fusion experiments, a $20Al(PO_3)_3$-80LiF-PrF_3 (Pr^{3+}-doped APLF) glass was irradiated with γ-rays from a cobalt-60 (^{60}Co) source resulting in an absorbed dose of 5.2 kGy. Although γ-ray-irradiation results in increased absorption due to phosphorus-oxygen hole centers (POHCs) and PO_3^{2-} electron centers (PO_3 ECs), these radiation-induced defects do not modify the glass emission as both non-irradiated and γ-ray-irradiated glasses exhibit similar emission spectra and decay times under optical and X-ray excitation. The emission peaks observed also correspond to the different interconfigurational $4f5d \rightarrow 4f^2$ and intraconfigurational $4f^2$ transitions of Pr^{3+} ions which are neither oxidized nor reduced by irradiation. Our results show that Pr^{3+}-doped APLF glass still maintains its characteristic fast decay time and that γ-ray irradiation does not affect the glass scintillation mechanisms. © 2022 The Japan Society of Applied Physics

1. Introduction

In inertial confinement fusion (ICF) research, neutron diagnostic techniques are very effective tools in examining fusion plasma dynamics. For the neutrons generated by the fusion reaction, the detection relies heavily on scintillator materials that contain neutron-sensitive elements such as lithium (^6Li), boron (^{10}B), and gadolinium (^{155}Gd, ^{157}Gd).[1)] Specifically, ^6Li scintillators are ideal for the measurement of 270 keV down-scattered neutrons to estimate the plasma areal density or measure the core shape asymmetry due to the large cross-section of ^6Li with the low-energy fast neutrons.[2–5)] However, while obtaining high ^6Li content, the scintillator material should also have good formation and chemical stability along with a high optical band gap or absorption edge. These requirements can be met by glasses that can be fabricated rapidly and economically into a variety of shapes, sizes, and chemical compositions.

Among the potential glass scintillator materials, the aluminum lithium fluorophosphate glass, $20Al(PO_3)_3$-80LiF (APLF) has been demonstrated to detect low-energy neutron signals when used as an array coupled to multi-anode photomultiplier tubes (PMTs).[6)] APLF has a lithium content of 31.6 mmol cm^{-3} comparable to that of the neutron scintillator, KG2 (36.0 mmol cm^{-3}) which has the highest ^6Li content of any commercially available Li glass scintillator.[7)] When doped with praseodymium (Pr^{3+}) ions, APLF is transparent to the interconfigurational $4f5d \rightarrow 4f^2$ emission of Pr^{3+} and exhibits sufficient scintillation yield of 310 photons with fast decay times of less than 6.0 ns under neutron excitation.[8,9)] These decay times are around 16 times faster than those of commercial cerium (Ce^{3+})-doped lithium silicate glasses—GS20 and KG2—which range from 93 to 98 ns under the same excitation.[10)] Since the time-of-flight (TOF) method is typically performed for particle discrimination, especially in ICF research, the high ^6Li content and the fast decay time are key quality criteria to enable the discrimination of the low-energy down-scattered neutrons from X-rays and primary neutrons generated by the fusion reaction.

Although APLF glass is considered a promising neutron scintillator material, little is known regarding the effects of radiation on the glass' structural, optical, and scintillating properties. Identifying the radiation effects is necessary because scintillators must also exhibit resistance in the presence of high-energy radiation.[11)] Several reports have already studied the effects of proton, X-ray, and gamma (γ)-ray irradiation on rare Earth ion-activated scintillator materials. For those doped with Pr^{3+} ions, however, most investigations focus on aluminum lutetium garnet ($Lu_3Al_5O_{12}$, LuAG) crystals grown by Czochralski[12–14)] and Bridgman methods,[11)] LuAG ceramics prepared by solid-state reaction,[15)] aluminum yttrium garnet ($Y_3Al_5O_{12}$, YAG) crystals also grown by Czochralski method,[14)] or silica glasses fabricated by sol–gel technique.[16)] Compared to crystals, glasses have more complex structures and may be prone to radiation leading to changes in chemical bonds and optical activator environment as well as defects leading to potentially induced optical absorption and emission decay time modification, among others. Therefore, it is vital to examine the effects of high-energy radiation for the scintillator application of APLF glasses inside future fusion reactors.

In this regard, we investigate the effects of γ-ray irradiation on Pr^{3+}-doped APLF glasses. Pr^{3+} is a very interesting optical activator as it exhibits multiple energy levels and a rich line emission spectrum that are strongly affected by the host matrix.[17–19] For instance, we have previously shown that Pr^{3+}-doped APLF glasses exhibit absorption and emission peaks which correspond to the various interconfigurational $4f5d \rightarrow 4f^2$ and intraconfigurational $4f^2$ transitions of Pr^{3+} ions usually located within different environments of the glass matrix.[20] Moreover, as high-energy photons, γ-rays can modify the population of electronic levels of existing defects or impurities, create new defects from knock-on collisions or radiolysis, and change the valence states of optical activators due to carrier capture.[15] A Pr^{3+}-doped glass is then irradiated with γ-rays with an absorbed dose of 5.2 kGy which is a modest value for the initial screening of fusion reactor components[21,22] but is relatively higher than or in the same range as those used in earlier investigations (10^0–10^3 Gy) on Pr^{3+}-doped scintillators.[11,13,14,23] Compared to other studies, Fourier transform infrared (FTIR) and X-ray absorption spectroscopies are also implemented since typical X-ray diffraction measurements cannot be performed on the amorphous glasses to evaluate their structure after irradiation. This work aims to compare the properties of the non-irradiated and γ-ray irradiated Pr^{3+}-doped APLF glasses, determine the effects of γ-ray irradiation on the glass properties, and obtain insights into the robustness of the fluorophosphate glass for future laser fusion experiments.

2. Experiment

2.1. Glass fabrication and irradiation

The Pr^{3+}-doped APLF glasses with nominal chemical compositions of $20Al(PO_3)_3$-80LiF-PrF_3 were prepared by the melt-quenching method described previously in Refs. 7,9,19,23–26. High-purity powders of aluminum metaphosphate [$Al(PO_3)_3$, 99.99%], lithium fluoride (LiF, 99.99%), 95 at % ^{6}Li-enriched LiF (99.6%), and praseodymium fluoride (PrF_3, 99.99%) were used as the raw materials. Mixed batches of each powder were melted in a glassy carbon (C) crucible with lid at 1000 °C for 30 min in nitrogen (N_2) atmosphere. The glass melts were then quenched at 400 °C and were annealed near the glass transition temperature of 340 °C. After being cooled to room temperature, the Pr^{3+}-doped APLF glasses were cut into 10.7 mm × 10.7 mm × 1.8 mm pieces and were polished on both sides to an optical finish. γ-ray irradiation was subsequently performed at the Rabbit11 facility of the Osaka University Institute of Scientific and Industrial Research (SANKEN).[27] The glasses were irradiated with γ-rays carrying 1.17 and 1.33 MeV energies from Rabbit11's cobalt-60 (^{60}Co) source which has a radioactivity of 21×10^{12} Bq. The estimated dose rate and total absorbed dose on the glass are 1.36 kGy h^{-1} and 5.2 kGy, respectively.

2.2. Glass characterization

Different spectroscopy techniques were conducted at room temperature to examine the non-irradiated and γ-ray-irradiated Pr^{3+}-doped APLF glasses. For the structural properties, the FTIR spectra were first measured using a JASCO FT/IR 6100 spectrophotometer with a single-reflection JASCO ATR-PRO410-S attenuated total reflection (ATR) accessory and diamond prism. Afterward, the X-ray absorption near edge structure (XANES) spectra for the Pr LIII edge were obtained in fluorescence yield mode at the BL-9A beamline of Photon Factory, High Energy Accelerator Research Organization (KEK), Tsukuba, Japan.[28] The I0 slit for the incident X-ray beam is 1.0 mm × 1.0 mm, and the full width at half maximum of the beam is about 500 μm × 300 μm. The energy was calibrated using the chromium (Cr) metal spectrum. Using a water-cooled Si (111) double-crystal monochromator, the photon energy which was calibrated using the chromium (Cr) metal spectrum was scanned from 5460 to 6460 eV, and the signals were recorded by a Lytle detector[29] with a vanadium (V) filter to reduce elastic scattering. All the experimental XANES data were analyzed using the Athena software.[30] For the optical properties, the absorption spectra from the UV to the NIR region were measured using a double-beam Hitachi U-4100 spectrophotometer. In addition, the emission spectra were obtained at the BL7B beamline of the Institute for Molecular Science Ultraviolet Synchrotron Orbital Radiation (UVSOR III) facility.[31] The glass sample was placed inside a vacuum chamber maintained at 10^{-6} Pa and was excited by wavelengths chosen using the beamline's 3 m normal incidence monochromator that has a dynamic range from 50 (VUV) to 1000 nm (IR). The glass emission was then fiber-fed to an Acton SpectraPro-300i spectrometer coupled to a liquid N_2-cooled PyLoN 400BR_eXcelon charge-coupled device (CCD) camera. Emission decay measurements were also implemented under the fourth harmonics (4ω, 217 nm) of a Spectra-Physics Ti:sapphire laser system operating with 100 fs pulse duration and 1 kHz repetition rate. The glass emission was focused on the entrance slit of a CHROMEX 250 is imaging spectrograph coupled to a Hamamatsu C4742-95 streak camera and a Hamamatsu C1587 CCD camera. Lastly, for the scintillating properties, the emission spectra were recorded under X-ray excitation from an Inel XRG 3000 X-ray source with a tungsten (W) anode set at 35 kV. The glass emission was detected using an Andor Shamrock SR500 imaging spectrometer coupled to an Andor Solis CCD-12570 camera. Emission decay measurements under X-ray excitation were likewise carried out using an X-ray tube set at 30 kV which was excited using a Horiba DD-405L light pulser set at 500 kHz. To select only the Pr^{3+} emission, a Thorlabs FGUV5M filter with a bandpass region of 240–395 nm and a maximum transmission of 87% was used.

3. Results

3.1. Structural properties

Figure 1 shows the photographs of the non-irradiated and γ-ray-irradiated Pr^{3+}-doped APLF glasses. The non-irradiated glass appears emerald green and transparent similar to other Pr^{3+}-doped glasses and crystals. In contrast, the γ-ray-irradiated glass is darker than its non-irradiated counterpart and appears slightly orange to brown.

Figure 2 shows the FTIR transmission spectra of the non-irradiated and γ-ray-irradiated Pr^{3+}-doped APLF glasses. Since the APLF glass is a system composed of $Al(PO_3)_3$ with a considerable amount of LiF and some PrF_3, multiple components such as the $P_2(O,F)_7$, $P(O,F)_4$, $(AlF_4)^-$, and $(AlF_6)^{3-}$ groups[32] contribute to the vibrational spectra alongside the

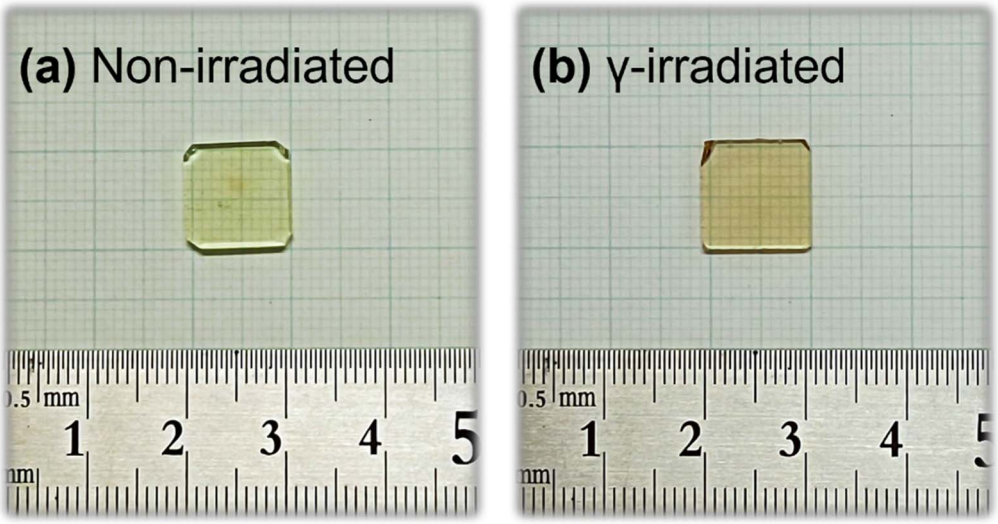

Fig. 1. (Color online) Photographs of non-irradiated and γ-ray-irradiated Pr^{3+}-doped APLF glasses.

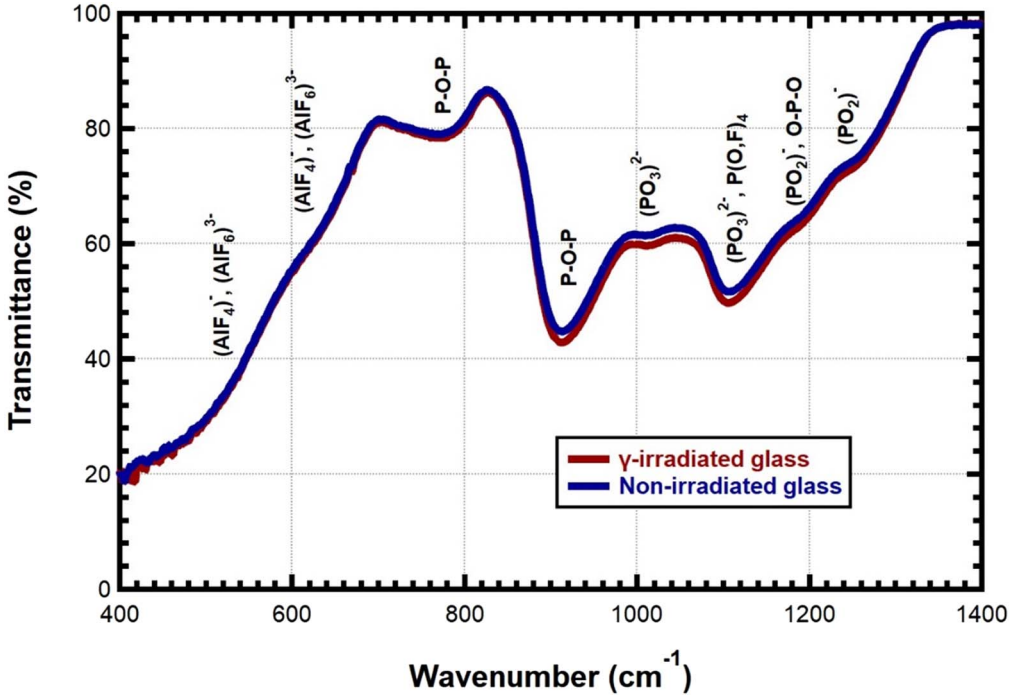

Fig. 2. (Color online) FTIR transmission spectra of non-irradiated and γ-ray-irradiated Pr^{3+}-doped APLF glasses.

typical $(PO_3)^{2-}$ and $(PO_2)^{-}$ groups.[33] The 564 and 668 cm^{-1} bands can be ascribed to the $(AlF_4)^{-}$ and $(AlF_6)^{3-}$ units as they appear in glass structures with relatively high metal fluoride components.[32] In addition, the bands located around 773 and 914 cm^{-1} correspond to the symmetric and asymmetric stretching of the P–O–P bridging oxygen chains, respectively. The P–O–P stretching vibrations are similarly observed in other fluorophosphate and phosphate glasses such as $2ZnO{\cdot}P_2O_5$-$2Na_2O{\cdot}P_2O_5$,[33] MnF_2-$NaPO_3$-ZnF_2,[34] $49.5P_2O_5$-$10AlF_3$-$10BaF_2$-$10SrF_2$-$10PbO$-$10Li_2O$-$0.5Pr_6O_{11}$,[35] $57.5Li_2O$-$5B_2O_3$-$37.5P_2O_5$-CeO_2,[36] and SnF_2-SnO-P_2O_5.[37] For APLF glass, in particular, the P–O–P stretching comes from the metaphosphate group and the pyrophosphate group, $P_2(O,F)_7$ that is present when the metaphosphate chains are shortened and when some oxygen atoms are replaced by fluorine atoms.[32] The band located around 1009 cm^{-1} is likewise associated with the symmetric stretching of the $(PO_3)^{2-}$ terminal group, while the 1106 cm^{-1} band is associated with the asymmetric stretching of the $(PO_3)^{2-}$ terminal group and the vibrations of some $P(O,F)_4$ groups that appear when the glass system has relatively low $Al(PO_3)_3$ content.[32] On the other hand, the 1181 cm^{-1} band is attributed to the O–P–O stretching of the $P_2(O,F)_7$ group along with the symmetric stretching of the $(PO_2)^{-}$ terminal group, while the 1244 cm^{-1} band is attributed to the asymmetric stretching of the $(PO_2)^{-}$ terminal group. Although the γ-ray-irradiated glass has slightly decreased transmittances (higher absorption) from 900 to 1250 cm^{-1}, this slight decrease is insignificant and does not indicate anything about the abovementioned bond groups. Hence, the non-irradiated and γ-ray-irradiated glasses exhibit similar IR absorption bands from 400 to 1400 cm^{-1}. This result suggests that γ-ray irradiation does not alter the structure of Pr^{3+}-doped APLF glass.

Figure 3 shows the XANES spectra of the non-irradiated and γ-ray-irradiated Pr^{3+}-doped APLF glasses for the Pr LIII edge. The spectra of PrF_3, Pr_2O_3, and Pr_6O_{11} standards are also plotted for reference. Both glasses exhibit identical spectral line shapes before and after the 5965 eV edge as well as the same white line intensities. The XANES spectra of the Pr^{3+}-doped APLF glasses also match those of the PrF_3 and Pr_2O_3 standards. These results suggest that the Pr ions exist in the APLF glasses with an environment similar to PrF_3 and Pr_2O_3 and an oxidation or valence state of +3. In addition, the non-irradiated and γ-ray-irradiated glasses do not exhibit any pre-edge peaks which can be attributed to any asymmetry or disorder of the atoms around the Pr^{3+} ions. These results reveal that γ-ray irradiation does not oxidize nor reduce Pr^{3+} ions and does not distort their arrangement in the APLF glass matrix.

3.2. Optical properties

Figure 4 shows the absorption spectra of the non-irradiated and γ-ray-irradiated Pr^{3+}-doped APLF glasses. Both glasses exhibit similar absorption edges and peaks from the UV to the visible region. The non-irradiated and γ-ray-irradiated glasses have absorption edges around 228 nm (5.44 eV, 43860 cm^{-1}) which correspond to the interconfigurational transition from the $^3H_4$ level of the $4f^2$ ground state configuration to the lowest level of the 4f5d excited state configuration of Pr^{3+} ions. The γ-ray-irradiated glass also exhibits absorption peaks identical to those of the non-irradiated glass, namely: 443 nm (2.80 eV, 22573 cm^{-1}), 468 nm (2.65 eV, 21368 cm^{-1}), 481 nm (2.58 eV, 20790 cm^{-1}), and 590 nm (2.10 eV, 16949 cm^{-1}) that correspond to the intraconfigurational $4f^2$ transitions of Pr^{3+} ions from the $^3H_4$ ground level to the higher $^3P_2$, $^3P_1 + {}^1I_6$, $^3P_0$, and $^1D_2$ levels, respectively. Shifting of the absorption edges and peaks is not observed between the non-irradiated and γ-ray-irradiated glasses. The only difference between both glasses is the gradual increase in absorption of the γ-ray irradiated glass from the visible (700 nm) to the UV (200 nm) region, which is likely related to a new absorption band and to its discoloration [Fig. 1(b)].

To further understand the increased absorption, Fig. 5 shows the differential absorption spectrum of the non-irradiated and γ-ray-irradiated Pr^{3+}-doped APLF glasses. The differential absorption or the radiation-induced absorption coefficient is calculated in the same manner as the procedure reported in Ref. 13. The resulting spectrum is then transformed into photon energy scale to allow a more convenient deconvolution into separate Gaussian components. Two Gaussian bands centered around 2.93 eV (423 nm, 23632 cm^{-1}) and 5.98 eV (207 nm, 48232 cm^{-1}) can be fitted to the radiation-induced spectrum. These 2.93 and 5.98 eV bands can be attributed to the radiation-induced defects or color centers, probably correlated to phosphorus-oxygen hole centers (POHCs) and phosphorus-related PO_3^{2-} (phosphoryl) electron centers (PO_3 ECs), respectively. Indeed, the visible-absorbing POHCs are single holes trapped on one or two non-bridging oxygen atoms bonded to the same phosphorus atom, while the UV-absorbing PO_3 ECs are single electrons trapped on three oxygen atoms bonded to one phosphorus atom.[38,39] These defects have also been observed from other phosphate glasses that were irradiated with γ-rays and X-rays and had similar increased absorption.[38–42] These results suggest that γ-ray irradiation induced some POHCs and PO_3 ECs acting as color centers in Pr^{3+}-doped APLF glass.

Figure 6 shows the emission spectra of the non-irradiated and γ-ray-irradiated Pr^{3+}-doped APLF glasses under 190, 200, and 220 nm synchrotron excitation. These excitation wavelengths have energies beyond the observed 228 nm absorption edge of the glasses (Fig. 4). Regardless of the excitation wavelength, both glasses exhibit overlapping emission spectra with similar line shapes and peak positions. In our previous work, we have reported that Pr^{3+} ions in APLF glass have a 4f5d excited state configuration (⩾ 5.39 eV, 43473 cm^{-1}) which overlaps with the $^1S_0$ level

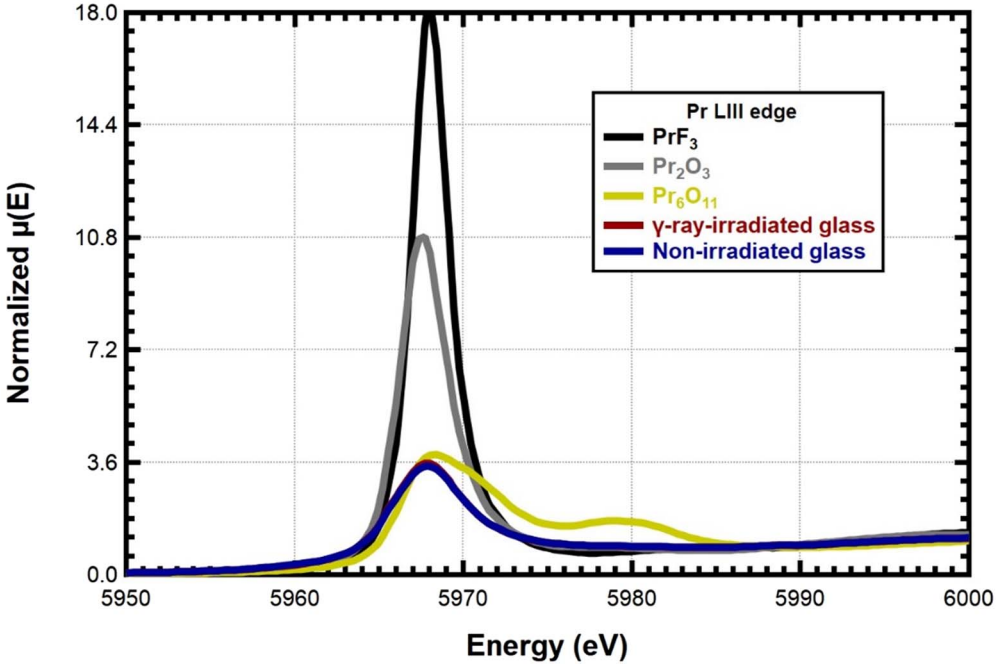

Fig. 3. (Color online) XANES spectra for the Pr LIII edge of non-irradiated and γ-ray-irradiated Pr^{3+}-doped APLF glasses.

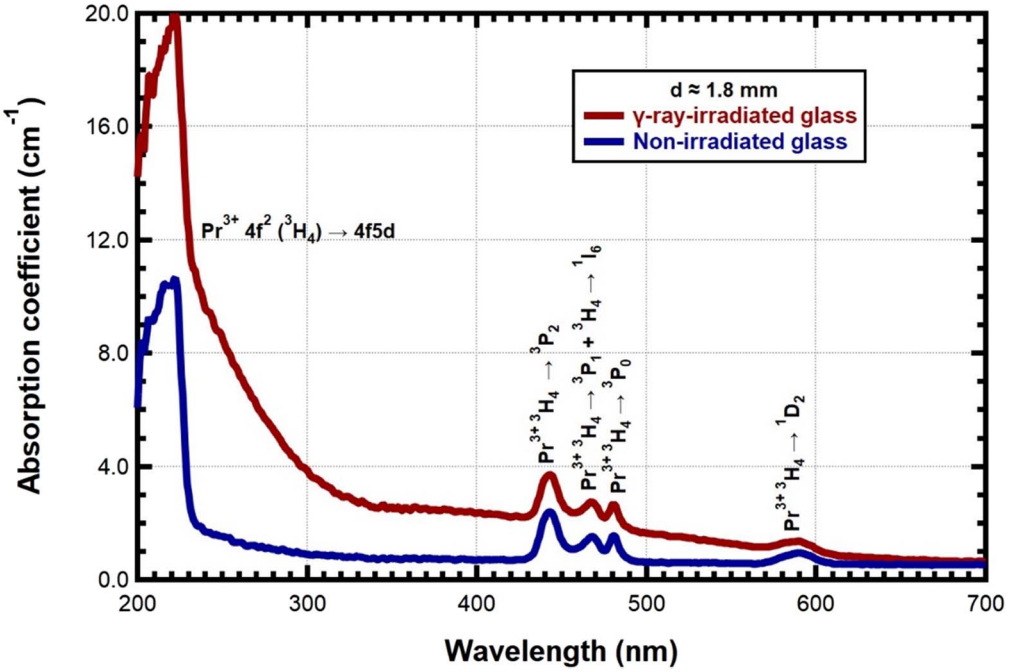

Fig. 4. (Color online) Absorption spectra of non-irradiated and γ-ray-irradiated Pr^{3+}-doped APLF glasses (thickness, $d \approx 1.8$ mm).

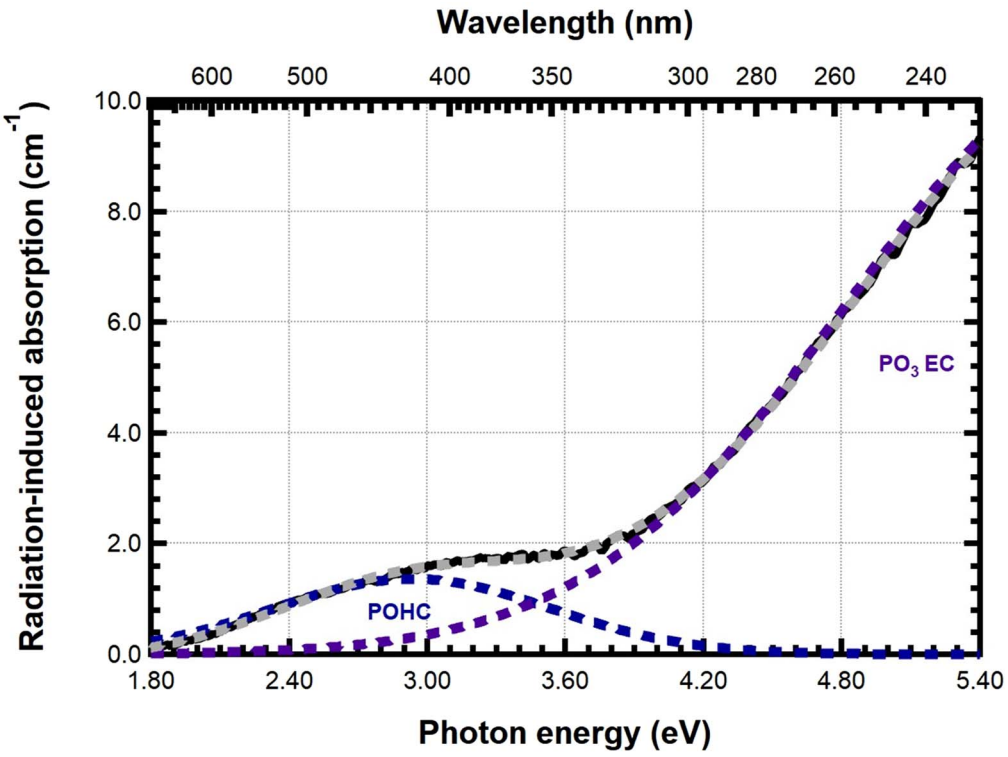

Fig. 5. (Color online) γ-ray radiation-induced absorption on Pr^{3+}-doped APLF glass.

($\sim$5.70 eV, 45974 cm^{-1}) of the $4f^2$ ground state configuration.[20] Hence, the 190 nm (6.53 eV, 52632 cm^{-1}) and 200 nm (6.20 eV, 50 000 cm^{-1}) excitation can excite both the 4f5d and $^1S_0$ levels, and the emission peaks and shoulders of the non-irradiated and γ-ray-irradiated glasses can be assigned to the interconfigurational $4f5d \rightarrow 4f^2$ and intraconfigurational $4f^2$ transitions of Pr^{3+} ions. In particular, the peaks located around 234 nm (5.30 eV, 42735 cm^{-1}) and 267 nm (4.64 eV, 37453 cm^{-1}) correspond to the interconfigurational transitions from the 4f5d configuration to the lower $^3H_5$ and $^3H_6$ energy levels of the $4f^2$ configuration, respectively. On the other hand, the peak around 257 nm (4.82 eV, 38911 cm^{-1}) corresponds to the intraconfigurational transition from the higher $^1S_0$ level to the lower $^3F_4$ level of the $4f^2$ configuration. In contrast, the 220 nm (5.64 eV, 45 455 cm^{-1}) excitation can only excite the 4f5d levels below the $^1S_0$ level. Therefore, the two interconfigurational $4f5d \rightarrow 4f^2(^3H_5)$ and $4f5d \rightarrow 4f^2(^3H_6)$ transitions are only observed with slightly shifted positions of 236 nm (5.25 eV, 42373 cm^{-1}) and 263 nm (4.71 eV, 38 023 cm^{-1}),

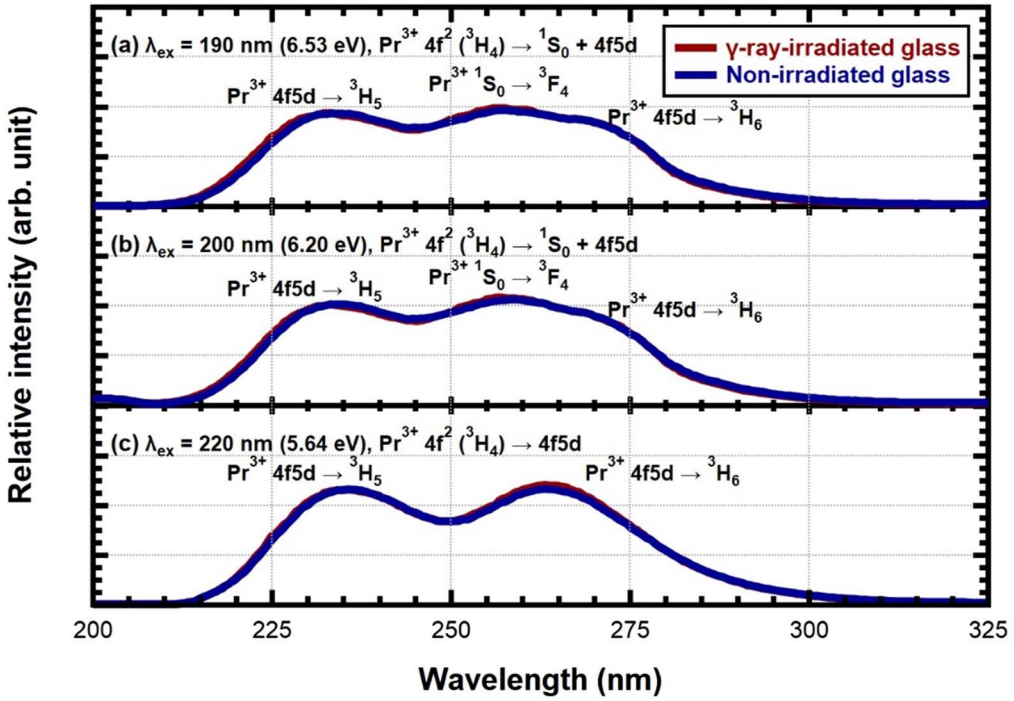

Fig. 6. (Color online) UV emission spectra of non-irradiated and γ-ray-irradiated Pr^{3+}-doped APLF glasses under (a) 190, (b) 200, and (c) 220 nm synchrotron excitation.

respectively. Since the difference in the peak intensities is also insignificant, the results indicate that γ-ray irradiation does not affect the UV emission of Pr^{3+}-doped APLF glass as the non-irradiated and γ-ray-irradiated glasses exhibit the same spectral properties regardless of the excitation wavelength.

Figure 7 shows the 267 nm emission decay profiles of the non-irradiated and γ-ray-irradiated Pr^{3+}-doped APLF glasses under 217 nm Ti:sapphire laser excitation. The 267 nm (4.46 eV, 37453 cm^{-1}) emission corresponds to the inter-configurational $4f5d \rightarrow 4f^2(^3H_6)$ transition of Pr^{3+} ions. Similar to the emission spectra (Fig. 6), both glasses exhibit overlapping profiles and the same characteristic exponential decay. By fitting a single exponential function on each profile, the non-irradiated and γ-ray-irradiated glasses are determined to have decay times of 18.5 and 18.1 ns, respectively. The difference in these decay times is within the 1.0 ns temporal resolution of the experimental setup. These results reveal that γ-ray irradiation does not modify the UV emission of Pr^{3+}-doped APLF glass and confirm that the Pr^{3+} local environment is the same between the non-irradiated and γ-ray-irradiated glasses.

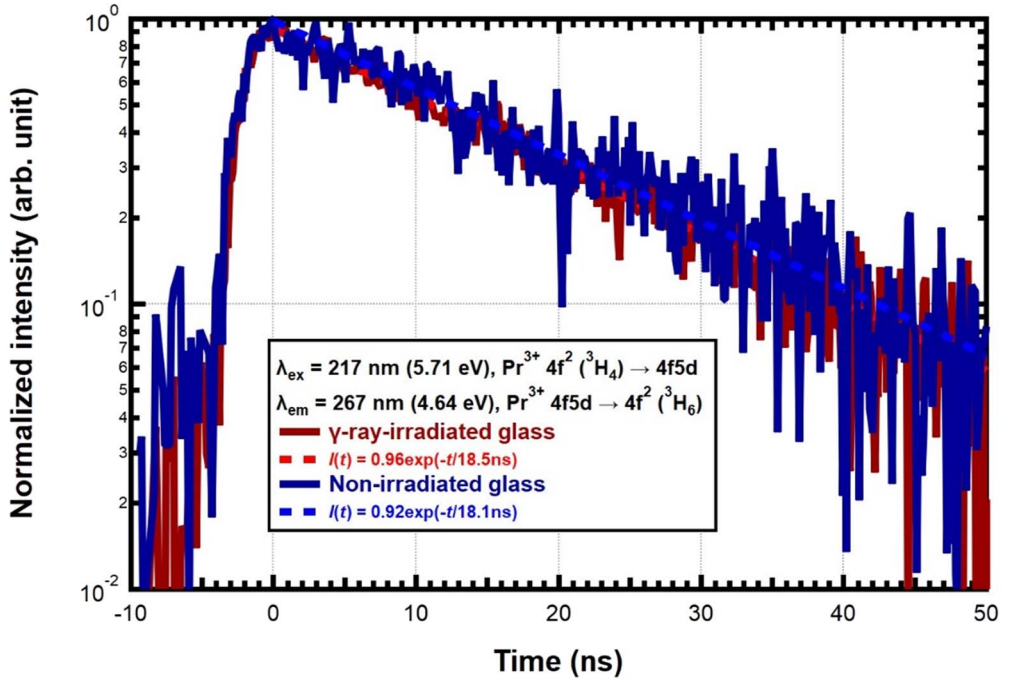

Fig. 7. (Color online) UV emission decay of non-irradiated and γ-ray-irradiated Pr^{3+}-doped APLF glasses under 217 nm Ti:sapphire laser excitation.

3.3. Scintillating properties

Figure 8 shows the emission spectra of the non-irradiated and γ-ray-irradiated Pr^{3+}-doped APLF glasses under X-ray excitation. Both glasses exhibit similar emission spectra from the UV to the visible region. In the UV region, the non-irradiated and γ-ray-irradiated glasses have broad and intense emissions with a peak around 267 nm (4.64 eV, 37453 cm^{-1}) and a shoulder around 238 nm (5.21 eV, 42 017 cm^{-1}). Similar to the emission spectra under different synchrotron excitation wavelengths (Fig. 6), these 238 and 267 nm emissions correspond to the interconfigurational transitions of Pr^{3+} ions from the 4f5d configuration to the lower $^3H_5$ and $^3H_6$ energy levels of the $4f^2$ configuration, respectively. A less intense UV emission peak around 360 nm (3.44 eV, 27 778 cm^{-1}) which corresponds to the interconfigurational 4f5d → $4f^2(^1D_2)$ transition can also be observed. In addition, the Pr^{3+}-doped APLF glasses exhibit six emission peaks located around 340 nm (3.65 eV, 29 412 cm^{-1}), 412 nm (3.01 eV, 24 272 cm^{-1}), 431 nm (2.88 eV, 23 202 cm^{-1}), 463 nm (2.68 eV, 21 598 cm^{-1}), 487 nm (2.55 eV, 20 534 cm^{-1}), and 530 nm (2.34 eV, 18 868 cm^{-1}) that correspond to the intraconfigurational $^1S_0 \rightarrow {}^1D_2$, $^1S_0 \rightarrow {}^1I_6$, $^3P_2 \rightarrow {}^3H_4$, $^1I_6 \rightarrow {}^3H_4 + {}^3P_1 \rightarrow {}^3H_4$, $^3P_0 \rightarrow {}^3H_4$, and $^3P_0 \rightarrow {}^3H_5$ transitions, respectively. Although the γ-ray-irradiated glass seems to have higher UV emission intensities compared to its non-irradiated counterpart, no significant differences in the emission intensities along with the peak positions and linewidths are observed between the non-irradiated and γ-ray-irradiated glasses. The relative intensities of both glasses are similar because the low-energy X-rays (30 keV) have a penetration depth in the order of 1.0 mm and the 2.93 and 5.98 eV absorption bands do not play a major role in the scintillation process (only a few cm^{-1}, Fig. 5). These results demonstrate that the γ-ray radiation-induced defects do not affect the energy transfer from the electron–hole pairs generated by the X-ray interaction to the Pr^{3+} ions in APLF glass.

Figure 9 shows the emission decay profiles of the non-irradiated and γ-ray-irradiated Pr^{3+}-doped APLF glasses under X-ray excitation. Since these decay profiles are measured using a filter with a bandpass region of 240–395 nm, the profiles are dominated by the glasses' intense Pr^{3+} 4f5d → $4f^2(^3H_6)$ emissions around 267 nm (Fig. 8). Both glasses exhibit very similar decay curves that can be fitted to an exponential function of the form:

$$I(t) = A_1 \exp\frac{-t}{\tau_1} + A_2 \exp\frac{-t}{\tau_2} + A_3 \exp\frac{-t}{\tau_3}, \qquad (1)$$

where I is the intensity, t is time, A_1, A_2, and A_3 are the numerical amplitudes, and τ_1, τ_2, and τ_3 are the decay constants. Aside from the overlapping decay curves, the non-irradiated and γ-ray-irradiated glasses exhibit similar decay constants (normalized amplitudes) of $\tau_1 = 0.64$ ns ($A_1 = 0.87$), $\tau_2 = 9.0$ ns ($A_2 = 0.13$), and $\tau_3 = 167$ ns ($A_3 = 0.07$). The 0.64 ns decay can be associated with the instrumental response, while the 167 ns decay can be considered a very weak afterglow. On the other hand, the 9.0 ns decay constants of the Pr^{3+}-doped APLF glasses are faster than the ones obtained from similar glasses (~19.6 ns) under optical excitation.[7,8] Under X-ray excitation, the APLF glass UV emission decay constants are also faster compared to other Pr^{3+}-doped glasses and crystals such as $20La_2O_3-30Al_2O_3-50B_2O_3$ (LAB, 15 ns),[43] $CaSiO_3$ (20 ns),[44] $Gd_2Si_2O_7$ (GPS, 18–29 ns),[45] $La_2Si_2O_7$ (LaPS, 25–27 ns),[46] and $SrLu_2O_4$ (14 ns).[47] It should be noted further that no additional slow component is observed on the γ-ray-irradiated glass as compared to its non-irradiated counterpart, i.e. both glasses have the same background which would increase in the presence of an additional slow component due to the X-ray excitation repetition rate. This result suggests that the radiation-induced defects do not play a role in the energy transfer during the fast scintillation of Pr^{3+}-doped APLF glasses.

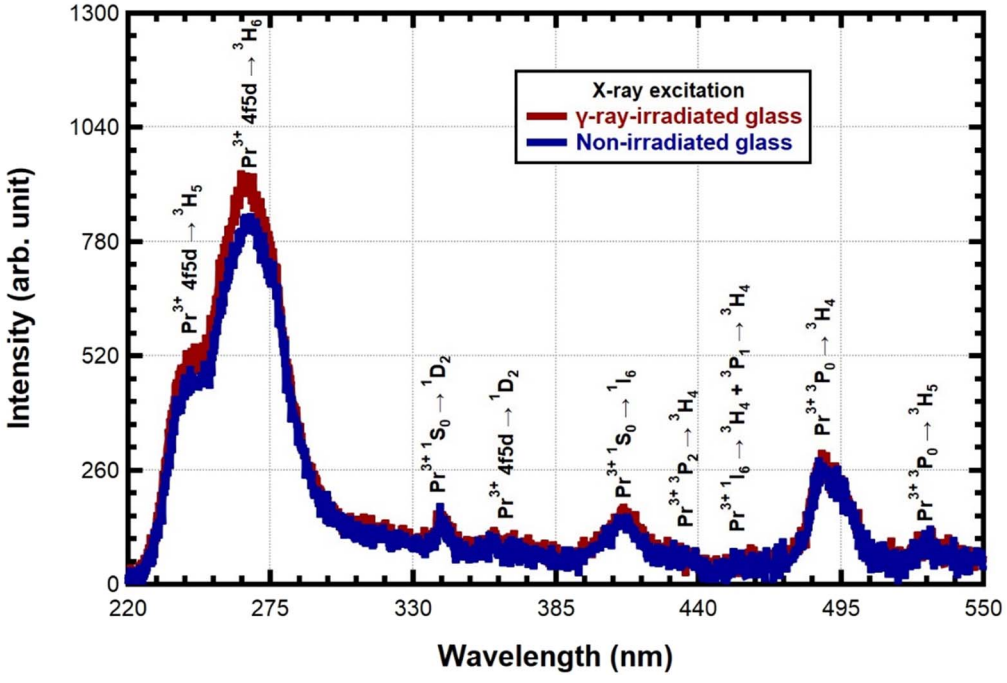

Fig. 8. (Color online) Emission spectra of non-irradiated and γ-ray-irradiated Pr^{3+}-doped APLF glasses under X-ray excitation.

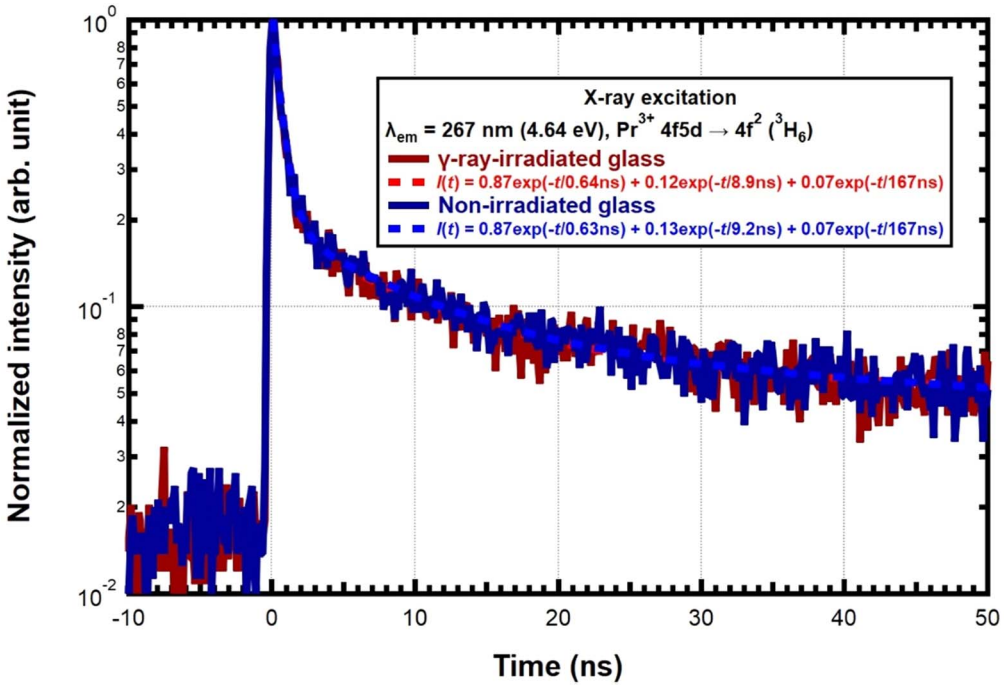

Fig. 9. (Color online) UV emission decay of non-irradiated and γ-ray-irradiated Pr^{3+}-doped APLF glasses under X-ray excitation.

4. Discussion

A γ-ray is a form of high-energy radiation that is known to affect the chemical, electronic, structural, and optical properties of materials. γ-ray radiation can convert pre-existing defects to color centers and can ionize or displace atoms generating electron and hole centers.[48] For instance, in Pr^{3+}-doped LuAG crystal, γ-ray irradiation leads to increased optical absorption with the appearance of bands peaking around 375 and 600 nm due to residual ytterbium (Yb).[11] Similarly, in Pr^{3+}-doped APLF glass, the irradiation results in discoloration (Fig. 1) and higher absorption (Fig. 4) due to the 2.93 eV (423 nm) and 5.98 eV (207 nm) bands (Fig. 5) attributed to radiation-induced POHCs and PO_3 ECs, respectively. However, the POHCs and PO_3 ECs cannot be associated with the glass structure since the non-irradiated and γ-ray-irradiated glasses exhibit similar IR transmittances (Fig. 2) and identical XANES spectra (Fig. 3). The structural properties of the Pr^{3+}-doped APLF glass are not significantly altered by γ-rays as the irradiation does not seem to break any bonds in the fluorophosphate glass as well as change the valence states and local environment of the Pr^{3+} ions. Moreover, the POHCs and PO_3 ECs do not modify the glass optical emissions that correspond to the interconfigurational $4f5d \rightarrow 4f^2$ and intraconfigurational $4f^2$ transitions of Pr^{3+} ions. Although the induced absorption overlaps with the emission spectrum, significant intensity losses due to reabsorption have not been observed even under different excitation sources. As shown in Figs. 6 to 9, the emission spectra and decay times of the Pr^{3+}-doped APLF glass are not affected by γ-ray irradiation which is very important for scintillator application. Hence, the presence of POHCs and PO_3 ECs cannot be regarded as radiation damage because the absorption due to these color centers does not affect the scintillation mechanism of the fluorophosphate glass. Furthermore, other phosphate glasses have been reported to recover from radiation-induced defects through thermal annealing and/or bleaching.[48] Additional investigations are then needed to elucidate the nature of the POHCs and PO_3 ECs, analyze the trapping of charge carriers, and examine the potential recovery of the fluorophosphate glasses. Taking everything into account, despite the presence of radiation-induced defects, the Pr^{3+}-doped APLF glasses can still be considered resistant to γ -ray radiation with robust emission properties suitable for scintillator application.

5. Conclusions

We have investigated the effects of γ-ray irradiation on Pr^{3+}-doped APLF glasses. By comparing the non-irradiated and irradiated glasses, it is confirmed that 5.2 kGy γ-ray irradiation does not alter the Pr^{3+} ion valence state and local environment. The γ-ray irradiation has only induced visible-absorbing POHCs and UV-absorbing PO_3 ECs that result in discoloration and increased absorption but do not affect the glass optical emissions, especially those that correspond to the interconfigurational $4f5d \rightarrow 4f^2$ transitions of Pr^{3+} ions in the UV region. Both non-irradiated and γ-ray irradiated glasses have similar emission peaks and intensities regardless of the excitation source. More importantly, the fast decay time of the fluorophosphate glass, i.e. < 20 ns under optical excitation and 9.0 ns under X-ray excitation, is not modified after irradiation. Therefore, γ-ray irradiation does not affect the crucial timing properties although it would probably affect the overall efficacy due to the transparency losses in real conditions. Nevertheless, as a potential scintillator material, Pr^{3+}-doped APLF glass is shown to have resistance to γ-rays and is acceptable for future laser fusion experiments.

Acknowledgments

This work was supported in part by the Japan Society for the Promotion of Science (JSPS) through Grant Nos.

JP22J11028, JP21K14562, and JP20K05091, by Tohoku University through the Global Institute for Materials Research Tohoku (GIMRT) Proposal No. 202112-RDKGE-0045, by the Osaka University Institute of Laser Engineering through the Collaborative Research Project No. 2022B1-004, and by Osaka University through the Research Abroad Program. The FTIR measurements were performed at the Analytical Instrument Facility of the Osaka University Graduate School of Science, while the X-ray absorption spectroscopy measurements were carried out under KEK Proposal Nos. 2021PF-T001 and 2022G030. The authors are likewise grateful to Ms. Youwei Lai, Mr. Haoze Yu, Mr. Shohei Tsurunaga, and Mr. Angelo P. Rillera for their assistance in the experiments.

ORCID iDs

Keito Shinohara https://orcid.org/0000-0003-3078-4902
Melvin John F. Empizo https://orcid.org/0000-0002-5660-9654
Marilou Cadatal-Raduban https://orcid.org/0000-0001-9641-132X
Masashi Yoshimura https://orcid.org/0000-0002-0770-1251
Nobuhiko Sarukura https://orcid.org/0000-0003-2353-645X
Mayrene A. Uy https://orcid.org/0000-0001-5379-1908
Hitoshi Abe https://orcid.org/0000-0001-6970-3642

1) J. P. Chaminade, O. Viraphong, F. Guillen, C. Fouassier, and B. Czirr, IEEE Trans. Nucl. Sci. **48**, 1158 (2001).
2) D. C. Wilson, W. C. Mead, L. Disdier, M. Houry, J.-L. Bourgade, and T. J. Murphy, Nucl. Instrum. Methods Phys. Res. A **488**, 400 (2002).
3) N. Izumi, R. A. Lerche, T. W. Phillips, G. J. Schmid, M. J. Moran, J. A. Koch, H. Azechi, and T. C. Sangster, Rev. Sci. Instrum. **74**, 1722 (2003).
4) M. Moran, S. Haan, S. Hatchett, J. Koch, C. Barrera, and E. Morse, Rev. Sci. Instrum. **75**, 3592 (2004).
5) J. A. Frenje et al., Rev. Sci. Instrum. **79**, 10E502 (2008).
6) Y. Arikawa et al., Rev. Sci. Instrum. **85**, 11E125 (2014).
7) T. Murata et al., IEEE Trans. Nucl. Sci. **57**, 1426 (2010).
8) Y. Arikawa et al., Rev. Sci. Instrum. **81**, 106105 (2010).
9) Y. Arikawa et al., Opt. Mater. **32**, 1393 (2010).
10) Saint-Gobain Crystals, Lithium Glass Scintillators, [https://www.crystals.saint-gobain.com/radiation-detection-scintillators/crystal-scintillators/lithium-glass-scintillators, (accessed 7 July 2022)].
11) M. V. Derdzyan, K. L. Ovanesyan, A. G. Petrosyan, A. Belsky, C. Dujardin, C. Pedrini, E. Auffray, P. Lecoq, M. Lucchini, and K. Pauwels, J. Cryst. Growth **361**, 212 (2012).
12) A. K. Islamov, E. M. Ibragimova, I. A. Khayitov, R. R. Vildanov, and K. N. Kudratov, Opt. Mater. **96**, 109344 (2019).
13) T. Iwashita and K. Miyabayashi, IEEE Nuclear Science Symp. & Medical Imaging Conf., 2010, p. 278 (Piscataway, NJ) (IEEE), 10.1109/NSSMIC.2010.5873764.
14) M. Nikl, E. Mihokova, V. Laguta, J. Pejchal, S. Baccaro, and A. Vedda, Proc. SPIE **6586**, 65860E (2007).
15) Y. Shen, X. Feng, Y. Shi, A. Vedda, F. Moretti, C. Hu, S. Liu, Y. Pan, H. Kou, and L. Wu, Ceram. Int. **40**, 3715 (2014).
16) F. Cova et al., J. Lumin. **192**, 661 (2017).
17) J. Legendziewicz, M. Guzik, J. Cybińska, A. Stefan, and V. Lupei, Opt. Mater. **30**, 1667 (2008).
18) J. Legendziewicz, M. Guzik, J. Cybińska, A. Stefan, and V. Lupei, J. Alloys Compd. **451**, 158 (2008).
19) P. A. Rodnyĭ, A. N. Mishin, and A. S. Potapov, Opt. Spectrosc. **93**, 714 (2002).
20) M. J. F. Empizo et al., J. Lumin. **193**, 13 (2018).
21) M. Malo, I. García-Cortés, P. Muñoz, A. Moroño, and E. R. Hodgson, Rev. Sci. Instrum. **89**, 065109 (2018).
22) M. Decreton, T. Shikama, and E. Hodgson, J. Nucl. Mater. **329–333**, 125 (2004).
23) A. G. Petrosyan et al., J. Cryst. Growth **430**, 46 (2015).
24) Y. Arikawa et al., Rev. Sci. Instrum. **80**, 113504 (2009).
25) M. Tsuboi et al., Jpn. J. Appl. Phys. **52**, 062402 (2013).
26) T. Murata et al., IOP Conf. Ser.: Mater. Sci. Eng. **18**, 112006 (2011).
27) Osaka University Research Laboratory for Quantum Beam Science, Institute of Scientific and Industrial Research, Research Laboratory for Quantum Beam Science, [https://www.sanken.osaka-u.ac.jp/labs/rl/English/index.html, (accessed 7 July 2022)].
28) KEK Photon Factory, BL9A High-intensity and Low-energy XAFS, [https://www.pfxafs.kek.jp/beamlies/bl-9a/, (accessed 7 July 2022)].
29) F. W. Lytle, R. B. Greegor, D. R. Sandstrom, E. C. Marques, J. Wong, C. L. Spiro, G. P. Huffman, and F. E. Huggins, Nucl. Instrum. Methods Phys. Res. A **226**, 542 (1984).
30) B. Ravel and M. Newville, J. Synchrotron Radiat. **12**, 537 (2005).
31) National Institutes of Natural Sciences Institute for Molecular Science, BL7B 3 m Normal-incidence Monochromator for Solid-state Spectroscopy, [https://www.uvsor.ims.ac.jp/beamlines/7B/bl7b.html, accessed 7 July 2022)].
32) F. Gan and H. Y. Chen, Mater. Sci. Forum **5–6**, 495 (1985).
33) A. M. Efimov, J. Non. Cryst. Solids **209**, 209 (1997).
34) T. Djouama, M. Poulain, B. Bureau, and R. Lebullenger, J. Non. Cryst. Solids **414**, 16 (2015).
35) S. Babu, P. Rajput, and Y. C. Ratnakaram, J. Mater. Sci. **5**, 8037 (2016).
36) Z. Zhang and W. Yang, Opt. Mater. Express **7**, 3979 (2017).
37) Y. Wang, Y. Yu, Y. Zou, L. Zhang, L. Hu, and D. Chen, RSC Adv. **8** 4921 (2018).
38) D. L. Griscom, E. J. Friebele, K. J. Long, and J. W. Fleming, J. Appl. Phys. **54**, 3743 (1983).
39) P. Ebeling, D. Ehrt, and M. Friedrich, Opt. Mater. **20**, 101 (2002).
40) P. Ebeling, D. Ehrt, and M. Friedrich, Phosphorus Res. Bull. **10**, 484 (1999).
41) G. Origlio, F. Messina, S. Girard, M. Cannas, A. Boukenter, and Y. Ouerdane, J. Appl. Phys. **108**, 123103 (2010).
42) J. A. Jiménez and C. L. Crawford, Opt. Mater. **127**, 112262 (2022).
43) S. Kaneko, H. Masai, G. Okada, N. Kawaguchi, and T. Yanagida, J. Asian Ceram. Soc. **5**, 385 (2017).
44) D. Nakauchi, G. Okada, M. Koshimizu, N. Kawaguchi, and T. Yanagida, Physica B **530**, 38 (2018).
45) P. Kantuptim, M. Akatsuka, D. Nakauchi, T. Kato, N. Kawaguchi, and T. Yanagida, Sensors Mater. **32**, 1357 (2020).
46) P. Kantuptim, T. Kato, D. Nakauchi, N. Kawaguchi, and T. Yanagida, Crystals **12**, 459 (2022).
47) H. Fukushima, D. Nakauchi, T. Kato, N. Kawaguchi, and T. Yanagida, Opt. Mater. **128**, 112385 (2022).
48) L. Petit, Int. J. Appl. Glas. Sci. **11**, 511 (2020).